Condensed [OPr4]10+ and Discrete [AsO3]3– Y1-Tetrahedra in Pr5O4Cl[AsO3]2

Hamdi Ben Yahia, Antoine Villesuzanne, Ute Ch. Rodewald, Thomas Schleid, Rainer Pöttgen

Condensed $[OPr_4]^{10+}$ and Discrete $[AsO_3]^{3-}$ Ψ^1-Tetrahedra in $Pr_5O_4Cl[AsO_3]_2$

Hamdi Ben Yahia[a], Antoine Villesuzanne[b], Ute Ch. Rodewald[a], Thomas Schleid[c], and Rainer Pöttgen[a]

[a] Institut für Anorganische und Analytische Chemie, Universität Münster, Corrensstraße 30, 48149 Münster, Germany
[b] CNRS, Université de Bordeaux, ICMCB, 87 avenue du Docteur Albert Schweitzer, 33608 Pessac Cedex, France
[c] Institut für Anorganische Chemie, Universität Stuttgart, Pfaffenwaldring 55, 70569 Stuttgart, Germany

Reprint requests to R. Pöttgen. E-mail: pottgen@uni-muenster.de

Z. Naturforsch. **2010**, *65b,* 549 – 555; received February 2, 2010

The oxide chloride arsenite $Pr_5O_4Cl[AsO_3]_2$ was obtained as green crystals as a by-product of the synthesis of PrO*T*As oxide arsenides (*T* = late transition metal), starting from Pr_6O_{11}, a transition metal oxide, arsenic, and an NaCl/KCl flux. $Pr_5O_4Cl[AsO_3]_2$ crystallizes with the monoclinic $Nd_5O_4Cl[AsO_3]_2$-type structure, space group *C*2/*m*. The structure was refined from single-crystal diffractometer data: a = 12.4943(15), b = 5.6884(13) c = 9.0776(19) Å, β = 116.61(1)°, $R(F)$ = 0.0264, $wR(F^2)$ = 0.0509, 542 F^2 values, and 52 variables. It is built up from corrugated layers of edge- and corner-sharing $[OPr_4]^{10+}$ tetrahedra, which are connected *via* chloride anions. The space between the layers is filled by these Cl^- and discrete arsenite anions $[AsO_3]^{3-}$ with lone pairs pointing towards each other. The network of condensed $[OPr_4]^{10+}$ tetrahedra is compared with the different arrays in the oxide pnictides α-PrOZnP, and in β-PrOZnP. Arsenic lone pair energy bands, main interactions, and the spatial distribution were identified precisely using density functional theory (DFT). Among the three crystallographically different sites for praseodymium, one was found non-magnetic in these calculations.

Key words: Oxide Chlorides, Oxoarsenites, Rare-earth Compounds, Crystal Structures

Introduction

Rare-earth metal(III) oxide pnictides *REOTPn* (*RE* = rare-earth element; *T* = late transition-metal; *Pn* = P, As, Sb) with the tetragonal ZrCuSiAs-type structure have attracted tremendous interest in the last two years due to their interesting magnetic, optical, and superconducting properties. Overviews are given in recent review articles [1 – 7]. Besides ceramic synthesis techniques starting from the rare-earth metal monopnictides and the transition metal oxides, various flux techniques, *i. e*. iron arsenide self-flux, tin flux, or halide flux mixtures, have been used for the growth of single crystals [2].

During our systematic studies of magnetic and optical properties of *REOTPn* materials [8 – 12] we repeatedly used NaCl/KCl fluxes for sample preparation. During synthesis attempts for PrORuAs [13] samples we obtained a by-product in the form of green transparent crystals. The structure determination reported herein has revealed that our by-product was $Pr_5O_4Cl[AsO_3]_2$. This oxide chloride arsenite is isotypic with the recently reported neodymium compound $Nd_5O_4Cl[AsO_3]_2$ [14].

Experimental Section

Synthesis

The title compound was first obtained as a by-product during synthesis attempts for PrORuAs for physical property measurements. $Pr_5O_4Cl[AsO_3]_2$ was then prepared by solid-state reaction from a mixture of re-sublimed arsenic (Sigma-Aldrich, > 99.999 %), praseodymium oxide Pr_6O_{11} (Chempur, Pr_6O_{11}, > 96 %) and a dried equimolar salt flux NaCl (Merck, > 99.5 %) / KCl (Chempur, > 99.9 %) with a 2:1:6 molar ratio. The mixture was put in an alumina tube, which was sealed under vacuum in a secondary silica tube. To ensure a total reactivity of the arsenic and to avoid its sublimation, the tube was heated at 500 °C for 24 h and at 600 °C

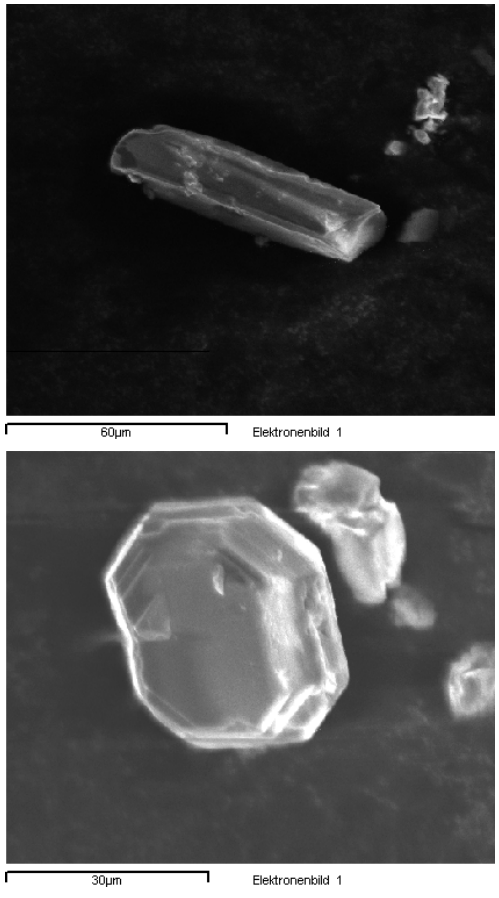

Fig. 1. SEM images of the $Pr_5O_4Cl[AsO_3]_2$ single crystal used for the XRD data collection (top) and the by-product PrOCl (bottom).

for 12 h, then annealed at 900 °C for 72 h. After washing the mixture with distilled water, we obtained a green powder, which mainly consisted of praseodymium sesquioxide (*A*-type). This powder was then mixed again with salt flux and heated at 850 °C for 4 d. With a relatively fast decrease of the temperature at a rate of 20 °C h^{-1} down to r. t., we obtained a few needle-shaped crystals of $Pr_5O_4Cl[AsO_3]_2$, which are transparent with green color. Oxidation of arsenic proceeds *via* Pr_6O_{11} with an almost fully tetravalent praseodymium content.

EDX data

Semiquantitative EDX analyses of many crystals including the one investigated on the diffractometer (Fig. 1) were carried out with a Leica 420i scanning electron microscope with PrF_3, GaP, and KCl as standards. The experimentally observed compositions were close to the composition obtained from the single-crystal refinement. On the surface of the crystals, some traces of sodium, potassium, and aluminum compounds which are due to the considerable reactivity of the alumina tube with the NaCl/KCl salt flux were observed.

Table 1. Crystallographic data and structure refinement for $Pr_5O_4Cl[AsO_3]_2$.

Formula	$Pr_5O_4Cl[AsO_3]_2$
Mw, g mol^{-1}	1049.8
Crystal color	green
Crystal shape	block
Temperature, K	293(1)
Crystal system	monoclinic
Space group	*C*2/*m*
Lattice parameters	
a, Å	12.4943(15)
b, Å	5.6884(13)
c, Å	9.0776(19)
β, deg	116.61(1)
V, nm^3	0.5768(2)
Z	2
F(000), e	916
Density calcd., g cm^{-3}	6.04
Diffractometer	Stoe IPDS II
Monochromator	oriented graphite
Radiation; λ, Å	MoK_α; 0.71073
Scan mode	multi-scan
hkl range	±18; ±8; ±12
θ_{min} / θ_{max}, deg	3.65 / 31.88
Linear absorption coeff., mm^{-1}	26.7
Absorption correction	Gaussian
T_{min} / T_{max}	0.309 / 0.748
No. of reflections	3548
No. of independent reflections	542
R_{int}	0.096
Reflections used [$I \geq 2\sigma(I)$]	419
Refinement	F^2
No. of refined parameters	52
R factors $R(F)$ / $wR(F^2)$	0.0264 / 0.0509
g. o. f.	0.85
Weighting scheme	$w = 1/(\sigma^2(I) + 0.0009I^2)$
Diff. Fourier residues, $e^-/Å^3$	−0.78 / +0.87

X-Ray diffraction

At each reaction stage, the polycrystalline sample was characterized by a Guinier pattern (imaging plate detector, Fujifilm BAS-1800) with Cu$K\alpha_1$ radiation and α-quartz (a = 491.30, c = 540.46 pm) as an internal standard. This allowed us to identify at least two phases. The major phase corresponds to the praseodymium sesquioxide (*A*-type), and the minor phases correspond to the title compound and PbFCl-type PrOCl. Both crystal types could be easily distinguished by their shape (Fig. 1).

A crystal suitable for single-crystal X-ray diffraction was selected on the basis of the size and the sharpness of its diffraction spots as obtained by Laue photographs on a Buerger camera (using 'white' Mo radiation). The data col-

Table 2. Atom positions and equivalent isotropic displacement parameters (U_{eq} in pm^2) for $Pr_5O_4Cl[AsO_3]_2$. U_{eq} is defined as one third of the trace of the orthogonalized U_{ij} tensor.

Atom	W.-position	*x* / *a*	*y* / *b*	*z* / *c*	U_{eq}
Pr1	2*a*	0	0	0	89(13)
Pr2	4*i*	0.25036(7)	0	0.86644(9)	67(2)
Pr3	4*i*	0.50029(5)	0	0.29295(5)	61(2)
Cl	2*c*	0	0	1/2	130(50)
As	4*i*	0.21599(13)	0	0.39048(14)	60(4)
O1	8*j*	0.1200(4)	0.2529(10)	0.9161(5)	71(14)
O2	4*i*	0.3569(7)	0	0.3961(8)	180(30)
O3	8*j*	0.3580(4)	0.2666(10)	0.7523(5)	88(15)

Table 3. Anisotropic displacement parameters (U_{ij} in pm^2) for $Pr_5O_4Cl[AsO_3]_2$. The anisotropic displacement factor exponent takes the form: $-2\pi^2[(ha^*)^2U_{11} + \ldots + 2hka^*b^*U_{12}]$.

Atom	U_{11}	U_{22}	U_{33}	U_{12}	U_{13}	U_{23}
Pr1	60(14)	110(20)	134(19)	0	77(12)	0
Pr2	53(3)	74(3)	80(3)	0	36(2)	0
Pr3	50(2)	75(3)	54(2)	0	20(2)	0
Cl	190(80)	20(8)	40(6)	0	−70(40)	0
As	44(6)	83(6)	32(4)	0	−2(4)	0
O1	42(19)	80(30)	91(15)	−6(17)	26(15)	31(16)
O2	90(30)	310(50)	120(30)	0	20(30)	0
O3	90(20)	60(20)	70(15)	10(2)	2(16)	14(15)

lection was then carried out on a Stoe IPDS II diffractometer using MoK_α radiation. Data processing and all refinements were performed with the JANA2006 program package [15]. A Gaussian-type absorption correction was applied, and the shape was determined with the video microscope of the Stoe CCD. Details about the data collection are summarized in Table 1.

Structure refinement

The extinction conditions observed for $Pr_5O_4Cl[AsO_3]_2$ were compatible with space group *C*2/*m*. The heavy-atom positions were found using the superflip program integrated in JANA2006 [15, 16]. The use of difference Fourier syntheses allowed us to localize the oxygen atom positions. With anisotropic displacement parameters for all positions, the residual factors converged to the values listed in Table 1. A literature search readily revealed isotypism with the recently reported neodymium compound $Nd_5O_4Cl[AsO_3]_2$ [14]. In the final cycles, the $Pr_5O_4Cl[AsO_3]_2$ structure was refined with the same setting. The refined atomic positions and anisotropic displacement parameters (ADPs) are given in Tables 2 and 3. Interatomic distances and bond valence sums [17] are listed in Table 4.

Further details of the crystal structure investigation may be obtained from Fachinformationszentrum Karlsruhe, 76344 Eggenstein-Leopoldshafen, Germany (fax: +49-7247-808-666; e-mail: crysdata@fiz-karlsruhe.de, http://www.fiz-informationsdienste.de/en/DB/icsd/depot_anforderung.html) on quoting the deposition number CSD-421438.

Computational details

Electronic structure calculations were achieved within density functional theory (DFT) and the all-electron, full-potential augmented plane wave plus local orbitals method (APW+lo) [18, 19], as implemented in the WIEN2K code [20]. The generalized gradient approximation (GGA) by Perdew, Burke and Ernzerhof [21] was used for the exchange-correlation energy. To account for the localized character of Pr-4*f* orbitals, a Hubbard *U* correction term was added according to the self-interaction corrected scheme (SIC) by Anisimov *et al*. [22], with parameters $U = 0.5$ Ryd and $J = 0.05$ Ryd. The plane-wave cutoff was set to $R_{MT} \times K_{max} = 7$, and a 24-points mesh was used to sample the irreducible wedge of the the Brillouin zone. Atomic sphere radii were set to 2.3 au, 2.5 au, 1.63 au and 1.65 au for Pr, Cl, As and O, respectively. The partition of the electron density was

Table 4. Interatomic distances (*d* in Å), angles (∠ in deg) and bond valence sums BVS [17] for $Pr_5O_4Cl[AsO_3]_2$. The coordination numbers are given in square brackets.[a]

	Distances	BV		Distances	BV
Pr1–O1 (4 ×)	2.434(6)	0.451	As–O2	1.739(9)	1.145
Pr1–O3 (4 ×)	2.528(4)	0.349	As–O3 (2 ×)	1.796(5)	0.984
	⟨2.481⟩	BVS [8] = 3.2		⟨1.777⟩	BVS [3] = 3.11
				angles	
Pr2–O1 (2 ×)	2.362(6)	0.544	O2–As–O3 (2 ×)	102.0(2)	
Pr2–O1 (2 ×)	2.373(5)	0.530	O3–As–O3	95.4(2)	
Pr2–O3 (2 ×)	2.536(6)	0.340		⟨99.8⟩	
	⟨2.424⟩	BVS [6] = 2.83			
Pr2–Cl	3.395(2)	0.091			
		BVS [7] = 2.92			
Pr3–O1 (2 ×)	2.298(5)	0.651			
Pr3–O2	2.364(10)	0.544			
Pr3–O3 (2 ×)	2.500(6)	0.375			
Pr3–O2	2.577(6)	0.304			
	⟨2.423⟩	BVS [6] = 2.9			
Pr3–Cl (2 ×)	3.410(1)	0.088			
		BVS [8] = 3.08			

[a] $BV = e^{(r0-r)/b}$ with the following parameters: $b = 0.37$, $r_0(Pr^{III}–O) = 2.138$, $r_0(As^{III}–O) = 1.789$ and $r_0(Pr^{III}–Cl) = 2.509$.

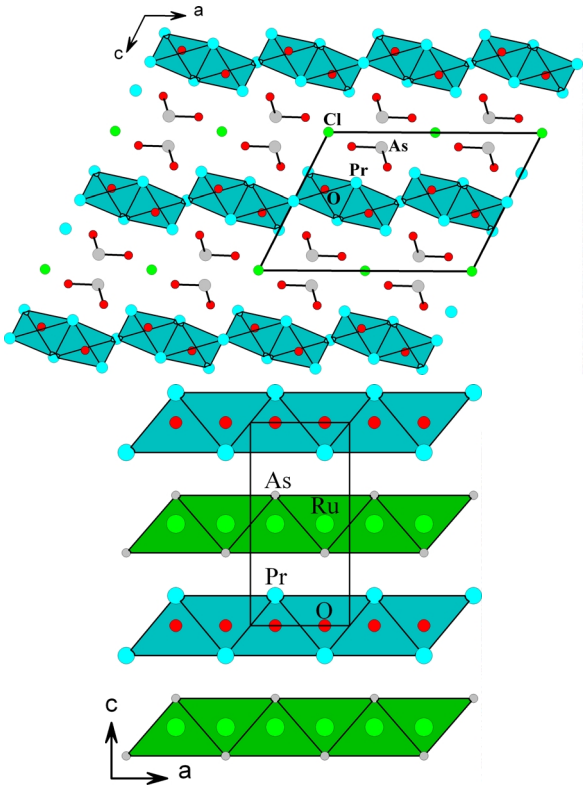

Fig. 2. Projection of the crystal structures of $Pr_5O_4Cl[AsO_3]_2$ (top) and PrORuAs (bottom) along the short unit cell axes (color online).

achieved according to Bader's "Atoms in Molecules" theory [23], as implemented in the WIEN2K code.

Discussion

$Pr_5O_4Cl[AsO_3]_2$ is isotypic with the recently reported neodymium compound $Nd_5O_4Cl[AsO_3]_2$ [14]. Due to the lanthanide contraction we observe slightly larger lattice parameters for the praseodymium compound. The striking structural motifs in the $Pr_5O_4Cl[AsO_3]_2$ structure are slightly distorted, oxygen-centered tetrahedra of praseodymium atoms with Pr–O distances ranging from 2.298 to 2.433 Å. As emphasized in Figs. 2 and 3, these $[OPr_4]^{10+}$ tetrahedra share common edges and corners in the *a* and common edges in the *b* direction, leading to corrugated layered networks.

Similar Pr–O distances occur in the two modifications of PrOZnP [8], *i. e.* 4 × 2.33 Å in α-PrOZnP (ZrCuSiAs type) and 1 × 2.36 and 3 × 2.39 Å in β-PrOZnP (NdOZnP type). In these oxide phosphides the $[OPr_4]^{10+}$ tetrahedra exclusively share common edges within planar layers, and they are well separated by the layers of likewisely edge-sharing $[ZnP_4]^{10-}$ tetrahedra. The different connectivity patterns of the $[OPr_4]^{10+}$ tetrahedra in α-PrOZnP, β-PrOZnP, and $Pr_5O_4Cl[AsO_3]_2$ are compared in Fig. 3.

The stacking of the different structural units of $Pr_5O_4Cl[AsO_3]_2$ and ZrCuSiAs-type PrORuAs [13] are presented in Fig. 2. In PrORuAs both isotopologically condensed layers of $^2_\infty\{[OPr_{4/4}]^+\}$ and $^2_\infty\{[RuAs_{4/4}]^-\}$ tetrahedra are planar, and consequently we observe a simple AB AB stacking sequence. In the $Pr_5O_4Cl[AsO_3]_2$ structure we have two different anionic units separating the layers of condensed $[OPr_4]^{10+}$ tetrahedra, *i. e.* chloride and arsenite anions. The Ψ^1-tetrahedral $[AsO_3]^{3-}$ units are arranged pairwise between the $[OPr_{4/4}]^+$ layers (Fig. 2). The lone pairs of the $[AsO_3]^{3-}$ anions point towards each other, and always two $[AsO_3]^{3-}$ units are related by a two-fold axis. To achieve a dense packing of these polyhedral units, a planar slab of condensed $[OPr_4]^{10+}$ tetrahedra is no longer possible. Thus we observe corrugated networks of edge- and corner-sharing $[OPr_4]^{10+}$ tetrahedra with the composition $^2_\infty\{[O_4Pr_5]^{7+}\}$ instead of $^2_\infty\{[OPr_{4/4}]^+\}$.

The three crystallographically independent praseodymium sites have coordination numbers of 7 or 8. The

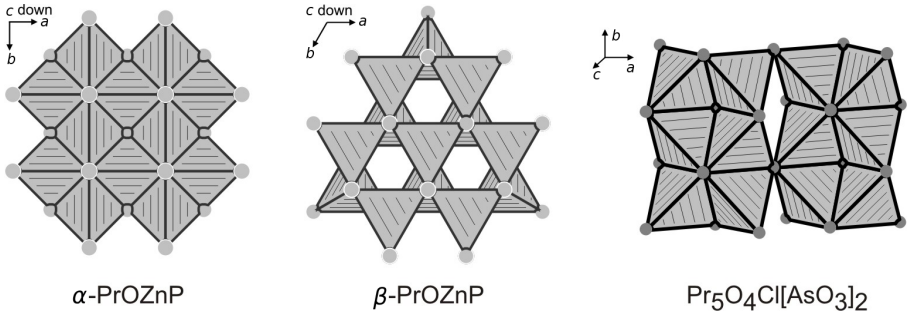

Fig. 3. The different condensation motifs of $[OPr_4]^{10+}$ tetrahedra in the structures of α-PrOZnP, β-PrOZnP, and $Pr_5O_4Cl[AsO_3]_2$. The motif observed for α-PrOZnP is also present in the chloride oxide PrOCl.

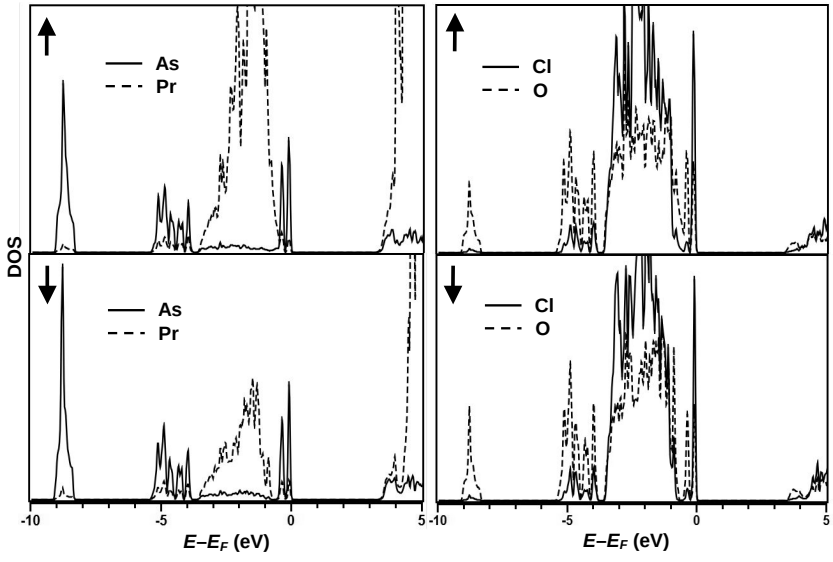

Fig. 4. Normalized partial density of states (DOS), calculated by the APW+lo/GGA+U method, for $Pr_5O_4Cl[AsO_3]_2$. Normalization was achieved by dividing the DOS values by the total multiplicity of each atomic species. Top: majority spin. Bottom: minority spin.

corresponding interatomic distances and bond valence sums [17, 24] are listed in Table 4. For further details concerning the coordination patterns we refer to the original work on the prototypic $Nd_5O_4Cl[AsO_3]_2$ [14].

Chemical bonding analyses

Fig. 4 shows the calculated spin-resolved density of states (DOS) for $Pr_5O_4Cl[AsO_3]_2$, using our crystallographic data as input. Pr-4*f* states largely dominate at the bottom of the conduction band, while the valence bands exhibit a much more hybridized character. The As-4*s* band is found around 9 eV below the Fermi level (E_F), strongly mixed with oxygen despite the rather low energy. The main valence band stack is divided into three blocks: i) O-2*p* states mixed with As-4*p* states lie within a 2 eV-wide energy range, around −4.5 eV, ii) the main body of the valence band, between −3.5 and −0.5 eV, has both Cl-3*p*, O-2*p* and Pr-4*f* character, and iii) a set of two very narrow bands between −0.5 eV and E_F, with Cl, As and O character.

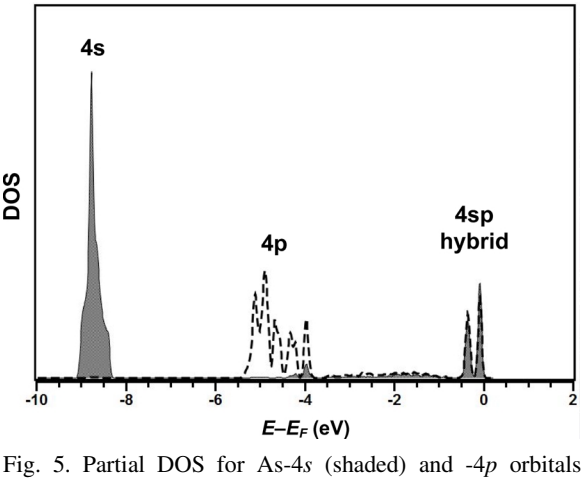

Fig. 5. Partial DOS for As-4*s* (shaded) and -4*p* orbitals (dashed line), calculated by the APW+lo/GGA+U method, for $Pr_5O_4Cl[AsO_3]_2$. Only one spin channel is shown, since majority and minority spin channels have almost identical As partial DOS.

As shown in Fig. 5, the As states are found apart of the valence band main body. The 4*s* character is naturally the main contribution to the band at −9 eV, but is also participating significantly in states close to the Fermi level. Thus, as seen in Fig. 5, the two narrow energy bands immediately below E_F correspond to a perfect hybridization of As-4*s* and -4*p* orbitals, *i. e.* a 4*sp* hybrid-orbital identified here as the As "lone pair". However, although the 4*sp* hybrid orbital contribution is unambiguously identified in these two bands below E_F, the partial DOS for O-2*p* (in both bands) and Cl-3*p* states (in the upper occupied band) is also significant; therefore, the 4*sp* lone pair is, in fact, strongly interacting with O-2*p* and Cl-3*p* orbitals.

As an illustration, Fig. 6 shows the calculated electron density in the *ac* plane ($y = 0$) for the two narrow bands below E_F. The signature of As-4*sp*, Cl-3*p* and O-2*p* orbitals is clearly visible, with comparable magnitudes, and shows clear antibonding 4*sp*-2*p* *versus* nonbonding 4*sp*-3*p* interactions. For the same bands, the

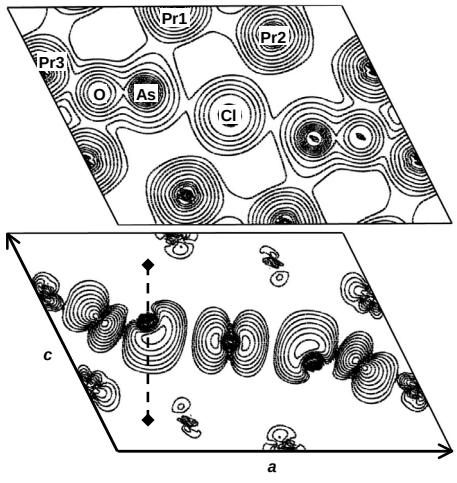

Fig. 6. Electron density isoline plots (logarithmic scale) in the *ac* plane (y = 0) calculated by the APW+lo/GGA+U method, for $Pr_5O_4Cl[AsO_3]_2$. Top: total electron density. Bottom: electron density for the two bands of As-4*sp* character, immediately below E_F. The 4*sp* orbitals interact in an antibonding manner with both O-2*p* and Cl-3*p* orbitals. Dashed line: projection of the perpendicular window used for the electron density plot in Fig. 7.

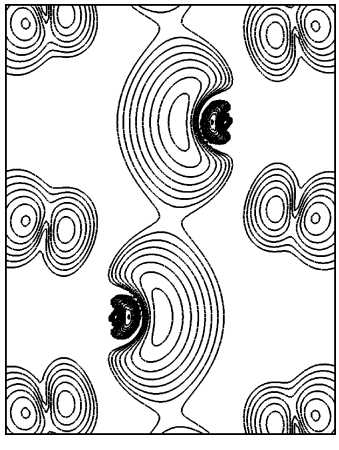

Fig. 7. Isoline plot (logarithmic scale) of the electron density in a plane perpendicular to (010), passing through two neighboring As atoms, for the two bands of As-4*sp* character ("lone pairs").

electron density in the plane perpendicular to the *ac* plane, and passing through As atoms (y = 0 and y = 1/2), shows an antiparallel, non-bonding arrangement of As-4*sp* hybrid orbitals (Fig. 7).

The plots of total electron density in the *ac* plane (y = 0) (Fig. 6) emphasizes the pronounced covalency of the As–O bonds. Pr–O interactions appear as slightly bonding, whereas the Cl atoms form very ionic bonds with both Pr and As atoms, as expected.

According to Bader's "Atoms in Molecules" theory [23], the atomic net charges are calculated by integration of the electron density in atomic basins, after identification of zero-flux surfaces of the density. This non-ambiguous partition procedure nonetheless leads to non-integral charges; the departure from formal charges roughly corresponds with the covalent character of the chemical bonding. Here, we found net charges of +2.1, +1.7, −0.8 and −1.3 $|q_e|$ for Pr, As, Cl and O, respectively. These charges are to be compared, for example, with those found for $Li_3[AsO_4]$ within the same calculation procedure: +0.90, +2.73, −1.35 for Li, As and O, respectively [25]. In $Pr_5O_4Cl[AsO_3]_2$, the Bader charges correspond to Pr^{3+}, As^{3+}, Cl^- and O^{2-}. The differences between Bader and formal charges correspond with the respective degrees of covalency of the As–O, Cl–O and Pr–O bonds seen from the electron density plots.

By integration of the partial DOS up to the Fermi level, net magnetic moments of 1.96, 1.96 and 0 μ_B found in Pr1, Pr2 and Pr3 atomic spheres, respectively. By adding the contribution of interstitial space, the Pr1 and Pr2 magnetic moments are expected to lie close to 3 μ_B. However, the striking fact that Pr3 is found non-magnetic remains an open issue; from the chemical bonding viewpoint, we did not find any specific features for the Pr3 site in this study. However, such behavior has been observed for $NdCo_2P_2$ [26], where every other neodymium layer shows no magnetic ordering.

Acknowledgements

This work was financially supported by the Deutsche Forschungsgemeinschaft. H. B. Y. is indebted to the Alexander von Humboldt Foundation for a research stipend.

[1] D. Johrendt, R. Pöttgen, *Angew. Chem.* **2008**, *120*, 4860; *Angew. Chem. Int. Ed.* **2008**, *47*, 4782.
[2] R. Pöttgen, D. Johrendt, *Z. Naturforsch.* **2008**, *63b*, 1135.
[3] H.-H. Wen, *Adv. Mater.* **2008**, *20*, 3764.
[4] T. C. Ozawa, S. M. Kauzlarich, *Sci. Techn. Adv. Mater.* **2008**, *9*, 033003.
[5] M. V. Sadovskii, *Physics–Uspekhi* **2008**, *51*, 1201.
[6] A. L. Ivanovskii, *Physics–Uspekhi* **2008**, *51*, 1229.

[7] Yu. A. Izyumov, E. Z. Kurmaev, *Physics–Uspekhi* **2008**, *51*, 1261.
[8] H. Lincke, T. Nilges, R. Pöttgen, *Z. Anorg. Allg. Chem.* **2006**, *632*, 1804.
[9] H. Lincke, R. Glaum, V. Dittrich, M. Tegel, D. Johrendt, W. Hermes, M. H. Möller, T. Nilges, R. Pöttgen, *Z. Anorg. Allg. Chem.* **2008**, *634*, 1339.
[10] I. Schellenberg, T. Nilges, R. Pöttgen, *Z. Naturforsch.* **2008**, *63b*, 834.
[11] M. Tegel, I. Schellenberg, R. Pöttgen, D. Johrendt, *Z. Naturforsch.* **2008**, *63b*, 1057.
[12] H. Lincke, R. Glaum, V. Dittrich, M. H. Möller, R. Pöttgen, *Z. Anorg. Allg. Chem.* **2009**, *635*, 936.
[13] P. Quebe, L. J. Terbüchte, W. Jeitschko, *J. Alloys Compd.* **2000**, *302*, 70.
[14] D.-H. Kang, J. Wontcheu, Th. Schleid, *Solid State Sci.* **2009**, *11*, 299.
[15] V. Petříček, M. Dušek, L. Palatinus, JANA2006, The Crystallographic Computing System, Institute of Physics, University of Prague, Prague (Czech Republic) **2006**.
[16] L. Palatinus, G. Chapuis, *J. Appl. Crystallogr.* **2007**, *40*, 786.
[17] I. D. Brown, D. Altermatt, *Acta Crystallogr.* **1985**, *B41*, 244.
[18] E. Sjöstedt, L. Nordström, D. J. Singh, *Solid State Commun.* **2000**, *114*, 15.
[19] G. K. H. Madsen, P. Blaha, K. Schwarz, E. Sjöstedt, L. Nordström, *Phys. Rev. B* **2001**, *64*, 195134.
[20] P. Blaha, K. Schwarz, G. K. H. Madsen, D. Kvasnicka, J. Luitz, WIEN2k, An Augmented Plane Wave Plus Local Orbitals Program for Calculating Crystal Properties, Vienna University of Technology, Vienna (Austria) **2001**.
[21] J. P. Perdew, K. Burke, M. Ernzerhof, *Phys. Rev. Lett.* **1996**, *77*, 3865.
[22] V. I. Anisimov, I. V. Solovyev, M. A. Korotin, M. T. Czyzyc, G. A. Sawatsky, *Phys. Rev. B* **1993**, *48*, 16929.
[23] R. F. W. Bader, H. Essén, *J. Chem. Phys.* **1984**, *80*, 1943.
[24] R. D. Shannon, *Acta Crystallogr.* **1976**, *A32*, 751.
[25] C. Frayret, C. Masquelier, A. Villesuzanne, M. Morcrette, J.-M. Tarascon, *Chem. Mater.* **2009**, *21*, 1861.
[26] M. Reehuis, P. J. Brown, W. Jeitschko, M. H. Möller, T. Vomhof, *J. Phys. Chem. Solids* **1993**, *54*, 469.